Published in final edited form as:
Cancer Discov. 2013 October ; 3(10): 1122–1129. doi:10.1158/2159-8290.CD-13-0330.

SF3B1 mutations are associated with alternative splicing in uveal melanoma

Simon J. Furney[1], **Malin Pedersen**[2], **David Gentien**[3,4], **Amaury G. Dumont**[3,5], **Audrey Rapinat**[3,4], **Laurence Desjardins**[3,6], **Samra Turajlic**[2], **Sophie Piperno-Neumann**[3,7], **Pierre de la Grange**[8], **Sergio Roman-Roman**[3,5], **Marc-Henri Stern**[#3,4], and **Richard Marais**[#1]

[1]The Cancer Research UK Manchester Institute, Wilmslow Road, Manchester M20 4BX, UK

[2]The Institute of Cancer Research, 237 Fulham Road, London SW3 6JB, UK

[3]Institut Curie, Paris, 75248 France

[4]Platform of Molecular Biology facilities, Translational Research Department, Institut Curie, Paris, 75248 France

[5]INSERM U830, Paris, 75248 France

[6]Department of Ophthalmological Surgery, Institut Curie, Paris, 75248 France

[7]Department of Medical Oncology, Institut Curie, Paris, 75248 France

[8]GenoSplice, Hopital Saint-Louis, Paris, 75010 France

[#] These authors contributed equally to this work.

Abstract

Uveal melanoma, the most common eye malignancy causes severe visual morbidity and is fatal in about 50% of patients. Primary uveal melanoma can be cured by surgery or radiotherapy, but the metastatic disease is treatment refractory. To understand comprehensively uveal melanoma genetics, we performed SNP arrays and whole genome sequencing on 12 primary uveal melanomas. We observed only ~2000 predicted somatic single nucleotide variants per tumor and low levels of aneuploidy. We did not observe an ultraviolet radiation DNA-damage signature, but identified *SF3B1* mutations in three samples and a further 15 mutations in an extension cohort of 105 samples. *SF3B1* mutations were associated with good prognosis and were rarely coincident with *BAP1* mutations. *SF3B1* encodes a component of the spliceosome and RNA sequencing revealed that *SF3B1* mutations were associated with differential alternative splicing of protein coding genes including *ABCC5* and *UQCC*, and of the long non-coding RNA (lncRNA) *CRNDE*.

Keywords

uveal melanoma; whole genome sequencing; *GNAQ*/*GNA11*; *SF3B1*

Corresponding authors: Richard Marais, The Cancer Research UK Manchester Institute, Wilmslow Road, Manchester M20 4BX, UK. Phone: +44(0)161 446 3100; Fax: +44(0)161 918 7491; rmarais@picr.man.ac.uk, Marc-Henri.Stern, Translational Research Department, Institut Curie, Paris, 75248 France. Phone: +33 (0)1 56 24 66 46; Fax: +33 (0)1 56 24 66 30; Marc-Henri.Stern@curie.fr.

Disclosure of Potential Conflicts of Interest
The authors declare no potential conflicts of interest.

Europe PMC Funders Author Manuscripts

Introduction

Uveal melanoma arises in the iris, cilliary body and choroid. Light skin complexion, fair hair, blue eyes and the presence of cutaneous nevi are risk factors in uveal melanoma (1), but the UVR-associated increase in cutaneous melanoma that occurred in countries such as Australia over the past 4 decades has not been accompanied by parallel increases in uveal melanoma (2–4). Thus the role of UVR in uveal melanoma etiology is unclear.

Class 1 uveal melanomas present a low risk of metastasis, whereas class 2 tumors are highly metastatic and are characterized by monosomy of chromosome 3 and gain of 8q. Mutually exclusive mutations in *GNAQ* or *GNA11*, the principal driver oncogenes in uveal melanoma, occur in ~85% of cases (5, 6), and inactivating mutations in the tumor suppressor *BAP1* occur in ~85% of metastatic tumors and are associated with disease dissemination (7). Recently, exome sequencing of uveal melanomas has identified recurrent mutations in *EIF1AX* and *SF3B1* (8, 9), predominantly in low grade tumors. Somatic mutations in *SF3B1*, which encodes a component of the spliceosome, also occur in hematological, breast and pancreatic cancers (10–13). Mutant *SF3B1* is associated with differential gene splicing in chronic lymphocytic leukemia (14), but aberrant splicing in *SF3B1* mutant uveal melanoma has not been reported (9).

To gain insight into uveal melanoma genetics, we performed SNP array analysis, whole genome sequencing, and RNA sequencing (RNA-seq) on 12 frozen primary uveal melanoma samples. Despite its dismal prognosis, we find that uveal melanoma has a remarkably low mutation burden, and we did not observe a UVR DNA-damage signature. However, we found recurrent mutations in *SF3B1* that were associated with differential alternative splicing of both coding and non-coding genes that may play a role in the etiology of this disease.

Results

Our discovery cohort comprised 12 primary uveal melanoma T3-T4 tumors that represented different histological types (1 epithelioid cell, 3 spindle cell and 8 mixed cases) and were treated by primary enucleation (Supplementary Table 1). One case was metastatic at diagnosis and 6 patients subsequently developed metastases. SNP array analysis was performed using Illumina HumanOmni2.5 SNP arrays and whole genome sequencing was performed on the Illumina HiSeq 2000 platform. The whole genome sequence coverage was >30× (Supplementary Table 2) and the data were aligned to the reference genome and duplicate reads excluded. The whole genomes were compared to their matched normal DNA to identify chromosomal translocations, short insertions/deletions (indels) and somatic single nucleotide variants (SNVs).

The SNP arrays revealed low levels of aneuploidy in 11 of the tumors and tetraploidy in tumor #7 (Supplementary Fig. S1; Supplementary Table 3). The diploid tumors presented recurrent chromosome 3 monosomy (9 tumors), losses of 1p (5 tumors), 6q (3 tumors) and 8p (5 tumors), and gains in 6p (4 tumors) and 8q (7 tumors; Supplementary Figs. S1, S2). These aberrations are characteristic of uveal melanoma, but we also observed loss of 16q in

three tumors and gain of chromosome 11 in two (Supplementary Figs. S1, S2). The presence of two identical copies of chromosome 3 in tumor #7 suggested that chromosome 3 monosomy preceded acquisition of the tetraploid state. Tumor #7 also displayed trisomy for 1q and monosomy for 8p. Commensurate with the SNP array data, whole genome sequencing also revealed a low level of chromosomal aberrations. We predicted 2-59 inter-chromosomal translocations, 0-7 intra-chromosomal translocations, no inversions, 2-25 large deletions and 0-5 large insertions (Supplementary Fig. S2; Supplementary Table 4). Thus, the frequency of structural variations in uveal melanoma is only ~40% of that reported in cutaneous melanoma and only ~20% of that reported in acral melanoma (Fig 1A)(15, 16). It is also only ~10% of that we recently found in mucosal melanoma (Fig. 1A) (17).

The whole genome sequencing also revealed a very low number of SNVs. We predicted only 1629-2604 (median 2112) somatic SNVs and 47-178 (median 67) somatic short indels (Table 1). The SNV mutation rate of <1 per Mb (Table 1) is markedly lower than is seen in most other types of cancer (Fig. 1B) and significantly lower than is seen in cutaneous (~30,000 mutations/genome), mucosal (~8000 mutations/genome), or acral (~5,000 mutations/genome) melanoma (15–17).

UVR-induced DNA damage is characterized by C>T transitions at the 3’ end of pyrimidine dinucleotides (18), a “signature” that accounts for 80-90% of mutations in cutaneous melanoma, and up to 60% of the mutations in acral melanoma (15, 16). Although C to T (G to A) transitions were the commonest mutation in uveal melanoma, they accounted for only ~35% of the lesions (Fig. 1C) and were not enriched at the 3’ position of pyrimidine dimers (Fig. 1D). Thus, UVR induced DNA damage does not appear to play a role in uveal melanomagenesis.

In line with the generally low level of mutations, we observed very few coding region mutations, predicting only 4-19 non-synonymous SNVs per tumor; of which 92% of those tested were validated by Sanger sequencing (Supplementary Table 5). We also predicted only 0-2 coding region indels per tumor (Table 1). The only recurrent mutations were A>T, p.209L mutations in *GNA11* (7 tumors) and T>A/T>G, p.209L mutations in *GNAQ* (3 tumors; Supplementary Table 6). We did, however, observe a small number of non-recurrent mutations in individual genes with possible functional significance, including C>T p.P107L in *GNA15* that was coincident with A>T, p.209L *GNA11* in tumor #10, C>T p.G8R in *EIF1AX* in tumor #8, and *BAP1* mutations in 7 tumors (Supplementary Table 6).

Critically, we also observed non-recurrent mutations in *SF3B1* in three tumors (T>G, p.K666T: tumor #6; T>C, p.K700E: tumor #11; C>T, p.R625H: tumor #12) and although there were no chromosome losses or gains in the region encoding *SF3B1* (2q33.1) these data suggested a role for *SF3B1* in uveal melanoma. We screened *SF3B1* in 105 additional consecutive archival primary uveal melanomas and detected 15 additional mutations (8 p.R625H, 4 p.R625C, 1 p.R625P, 1 p.R625L, 1 p.K666T; Supplementary Table 7). Our overall mutation rate of 15% (18/119) is similar to the rate (18.6%) recently reported for *SF3B1* mutations in uveal melanoma by whole exome sequencing (9), but note that in addition to the R625 codon mutations reported therein, we also observed K666 and K700 codon mutations (Supplementary Fig. S3). The *SF3B1* mutations are inversely associated

with chromosome 3 monosomy and notably, they are associated with improved progression-free and cancer survival (Supplementary Table 7, Supplementary Fig. S4).

SF3B1 encodes subunit 1 of splicing factor 3b, a component of the spliceosome, so to evaluate the effects of *SF3B1* mutations on uveal melanoma transcripts, we hybridized three *SF3B1* mutated tumors and three *SF3B1* wild-type tumors to Affymetrix Human Transcriptome Arrays (HTA2), which contain both exon and exon-exon junction probes. 325 genes were predicted to be differentially expressed, with 46 genes up-regulated and 279 genes down-regulated in the *SF3B1* mutant compared to the *SF3B1* wild-type tumors (Supplementary Table 8). Gene Ontology (GO) and pathway analysis of the differentially expressed genes did not predict any significant GO term(s), and did not predict KEGG or REACTOME pathway enrichment. However, splicing level analysis predicted 130 genes that contained at least one differentially regulated exon and/or splicing pattern (Supplementary Table 9). Manual inspection of the predicted events by the GenoSplice EASANA® visualization interface revealed eight high-confidence or very high-confidence events, including alternative terminal exons (four events), alternative 3' acceptor splice sites (two events), alternative cassette exons (one event), and intron retention (one event; Table 2). Critically, six of these events (*GUSBP11, UQCC, ANKHD1, ADAM12, CRNDE* and *ABCC5*) were also identified when we analyzed the RNA-seq data from Harbour *et al.* (Table 2).

Next, we compared the RNA-seq data from our three *SF3B1* mutant to our nine *SF3B1* wildtype tumors. For this we used DEXSeq, a Bioconductor package that uses generalized linear models to detect differential exon usage (19), and also MATS, which uses a Bayesian statistical framework to identify alternative splicing (20). 47 genes were predicted to be differentially spliced in these two populations by at least one algorithm (Supplementary Tables 10 & 11). Strikingly, when we compared our analysis of our HTA2 and the Harbour *et al.* data with our RNA-seq analyses, three alternative splicing events, *CRNDE, ABCC5* and *UQCC*, were identified by all three analyses (Table 2). These data suggest that *CRNDE, ABCC5* and *UQCC* are strong candidates for alternative splicing in *SF3B1* mutant tumors, hence we examined the sequencing profiles for three genes in our RNA-seq data. We normalized the number of mapped bases for these genes and compared nucleotide coverage at each base in *SF3B1* mutant and wild-type tumors (Fig. 2).

The profiles for *UQCC*, revealed clear evidence of alternative terminal exon use in the *SF3B1* wild-type and *SF3B1* mutant tumors (Fig. 2A). For *CRNDE* we observed near uniform representation of all bases of exon 4 in the *SF3B1* wild-type tumors, but an enrichment of the reads at the 3' end of this exon in the *SF3B1* mutant tumors (Fig. 2B). Finally, in ABCC5, we observed clear evidence of differential splicing of intron 8 (Fig. 2C). Critically, we detected all three of these splicing events when we analysed the RNA-seq data from Harbour *et al* (Supplementary Figure S5)(9) providing independent confirmation of these alternative splicing events.

Finally, to further validate our findings, we assessed alternative splicing of *GUSBP11, UQCC, ANKHD1, GAS8, F8, ADAM12, CRNDE and ABCC5* – the eight genes that provided the strongest evidence of splicing – by qRT-PCR in 74 independent uveal

melanomas comprising 58 *SF3B1* wild-type and 16 *SF3B1* mutant tumors. This analysis confirmed that all eight genes were alternatively spliced in *SF3B1* mutant compared to *SF3B1* wild-type tumors (Fig. 2D, Supplementary Fig. S6).

Discussion

We describe here the first whole genome sequencing of uveal melanoma, and our data reveal that this is a comparatively simple genetic disease characterized by recurrent chromosomal gains and losses and a relatively low number of SNVs and structural variants. The tumor genomes display a homogenous SNV burden, both in terms of number (1629-2604) and mutation class, and notably, they do not display a canonical UVR-induced DNA damage signature at pyrimidine dinucleotides. The absence of this signature negates an obvious influence of UVR in the etiology of this disease.

We confirm that *GNAQ* and *GNA11* are the most commonly mutated driver oncogenes and that *BAP1* is the most commonly mutated tumor suppressor. In addition, we confirm *SF3B1* as recurrently mutated in 15% of cases, with a mutation hotspot at codon R625. *SF3B1* mutations have been reported in hematological, breast and pancreatic cancers (10–13). Intriguingly, in those cancers codon K700 mutations predominate whereas in uveal melanoma R625 codon mutations predominate. This suggests that either the gene mutations have distinct etiology, so different hotspots are targeted in each disease, or that the diverse biology of the diseases favors selection of discrete mutations. Notably, in common with previous studies (8, 9), we confirm that in uveal melanoma *SF3B1* mutations are associated with better prognosis. Thus, in uveal melanoma and myelodysplastic syndrome SF3B1 mutations are associated with improved outcome, whereas in chronic lymphocytic leukemia (CLL), *SF3B1* mutations are associated with poorer prognosis (21).

SF3B1 encodes subunit 1 of splicing factor 3b, a component of the spliceosome, a large intracellular machine that processes precursor mRNA into mature transcripts. Specifically, splicing factor 3b anchors precursor mRNA onto the splicosome to define the splicing site. Previous studies show that spliceosomal component mutations can alter splicing within a gene, can cause intron retention or can cause aberrant alternative splicing, affecting protein isoform balance and thereby cell proliferation and differentiation (22, 23). In CLL, *SF3B1* mutations are associated with alternative splicing at the 3’ ends of genes to generate truncated variants of the vitamin C transporter *SLC23A2*, the T-cell regulator *TC1RG1*, and the forkhead transcription factor *FOXP1*. We show that in uveal melanoma *SF3B1* mutations are also associated with alternative splicing (Fig. 2D). We show that in common with CLL, *SF3B1* mutations in uveal melanoma are associated with alternative splicing of the 3’ end of transcripts, for example in *UQCC*, which encodes the ubiquinol-cytochrome c reductase complex chaperone, a protein implicated in bone development and stature. We also see differential splicing of *ABCC5*, a multidrug resistance-associated protein that is implicated in breast cancer metastasis (24) and colorectal cancer (25). Interestingly, in uveal melanoma, we observe evidence of intron retention in *ABCC5* in the *SF3B1* wild type samples compared to the mutant samples, suggesting that this gene is more efficiently spliced in the *SF3B1* mutant than wild-type tumors.

More intriguing, we show that *SF3B1* mutations are associated with cryptic alternative splicing of exon 4 of *CRNDE*. This long non-coding RNA (lncRNA) exists in several alternatively spliced forms and is upregulated in both solid tumors and leukemias (26, 27). *CRNDE* in general, and exon 4 in particular is alternatively spliced in colorectal cancer and the alternative forms are thought to regulate gene expression by regulating chromatin-modifying enzymes (27, 28). We show that in uveal melanoma, mutations in *SF3B1* are associated with cryptic alternative splicing within exon 4 of *CRNDE*, and considering the comparatively simple genetics of uveal melanoma, it will be important to determine how alternative splicing of this non-coding gene affects cellular function.

In conclusion, we show that despite its appalling prognosis, uveal melanoma is a relatively simple genetic disease characterized by recurrent chromosomal losses and gains, and a low mutational burden. We confirm that *GNAQ*/*GNA11* are the most commonly mutated oncogenes and *BAP1* the most commonly mutated tumor suppressor. We identify *SF3B1* mutations in ~15% of cases and show these are associated with better prognosis, which will guide clinical management of this disease. Intriguingly, we show that *SF3B1* mutations are associated with diverse alternative splicing events, including alternative terminal exon usage, intron retention and cryptic splicing within exons of both protein coding and non-coding genes. Future studies will focus on how these events affect uveal melanoma biology.

Methods

Patient Cohorts

Discovery set—Twelve patients with uveal melanoma were included in the WGS study (Supplementary table 1) from whom tumour and matched blood samples were obtained. This study was approved by the ethics committee of Institut Curie and informed consent was obtained from all subjects.

Validation set—Consecutive patients diagnosed at the Institut Curie between January 2006 and December 2008 who underwent primary enucleation and with sufficient material at the Biobank were included in the validation series with exclusion of patients with metastasis at diagnosis. Patient characteristics are reported in Supplementary table 6. The follow-up for this analysis ended on December 2012, with a median time of 38 months. During this period, 57 patients (53%) developed metastatic disease and 50 patients (47%) died. Metastatic melanoma was the cause of the death in 43 patients (40%). DNA was extracted from frozen materials or FFPE sections. *SF3B1, GNAQ, GNA11* and *BAP1* were sequenced by Sanger methods. Oligonucleotide primer sequences are available upon request.

DNA and RNA extraction and sequence analysis

Tumor DNA and RNA were provided by the Biological Resource Center of the Institut Curie. The DNA was extracted from frozen tumor or formalin-fixed paraffin-embedded samples using a standard phenol/chloroform procedure. The total RNA was isolated from frozen tumor samples using TRIzol reagent and cDNA synthesis was performed with MuLV Reverse Transcriptase in accordance with the manufacturers' instructions (Invitrogen, Cergy-Pontoise, France), with quality assessments performed on an Agilent 2100 bioanalyzer. For

Sanger sequencing, gDNA was amplified by PCR and the products were sequenced using dye-terminator chemistry as previously described (16). Primer sequences are available upon request. Sequences were visualized using Sequencher software.

Whole genome sequencing and analysis

Extracted DNA samples were sequenced on three lanes of Illumina Hiseq2000 sequencers to produce paired-end reads of 100bp. FASTQ files from each lane were aligned to the human reference genome (GRCh37). Data for each sample were merged and duplicate reads were marked using Picard (http://picard.sourceforge.net/). Somatic variants were identified by comparing matched tumor and normal genomes (Supplementary Methods).

SNP array analysis

Genome-wide genotyping for tumor and blood DNA samples was conducted on Illumina HumanOmni2.5 SNP arrays. Raw data files were processed using GenomeStudio and somatic alterations were identified (Supplementary Methods).

RNA extraction and Array hybridization

Total RNA was isolated from frozen biopsy using a miRNeasy mini kit (Qiagen) and quality assessment was conducted using RNA 6000 Nano labchip (Bioanalyzer, Agilent) and by a Nanodrop spectrophotometer (Thermo). Total RNA RIN values were between 7.7 and 9 (average: 8.65). Affymetrix Human Transcriptome Array 2.0 ST arrays were hybridized according to Affymetrix recommendations using the Ambion WT protocol (Life technologies, France) and Affymetrix labeling and hybridization kits. 100ng of total RNA were processed in parallel with an external MAQC A RNA to control robustness of data. Labeled DNA mean yield was 7.19 µg (min: 6.27µg; max: 7.57µg). Affymetrix GeneChip® Human Transcriptome 2.0 ST microarrays (HTA2) were hybridized with 4.7 µg of labeled DNA. Raw data, transcript data and exon data were controlled with Expression console (Affymetrix) at the Institut Curie microarray core facility. The benefit of this array is to highlight spliced RNA isoforms using both exon and exon-exon junction probes that can measure excluded or included exons/regions.

Microarray data analysis

Affymetrix HTA2 dataset analysis was performed by GenoSplice technology (www.genosplice.com and Supplementary Methods). We performed an unpaired Student's t-test to compare gene intensities between *SF3B1* wild-type and *SF3B1* mutated tumors. Genes were considered significantly differentially expressed when fold-change was ≥1.5 and P-value ≤0.05 (unadjusted P-value). Analysis at the splicing level was first performed taking into account only exon probes ('EXON analysis'; see Supplementary Methods). Results were considered statistically significant for unadjusted P-values ≤ 0.05 and fold-changes ≥ 1.5 for SPLICING PATTERN analysis and unadjusted P-values ≤ 0.05 and fold-changes ≥ 2.0 for EXON analysis. After bioinformatics analysis of microarray data, a manual inspection using the GenoSplice EASANA® interface was conducted to select high-confident events.

RNA-seq analysis

RNA from the 12 tumor samples was sequenced (Supplementary Methods). Reads were aligned using Tophat (29). Differential splicing analysis between the mutant (n=3) and wild-type *SF3B1* (n=9) samples was conducted using DEXseq (19) and events with an FDR <0.1 were regarded as significant. Differential splicing analysis was also conducted by MATS (20), using the mapped read bamfiles as input and events with an FDR <0.1 were regarded as significant. The RNA-seq data from the Habour *et al.* study (9) were downloaded from the NCBI Sequence Read Archive (http://www.ncbi.nlm.nih.gov/sra?term=SRA062359) and analysed using the same methodology with the exception that read lengths were trimmed to 99bp. One of the samples described as wild-type *SF3B1* was predicted to have an *SF3B1* R625C mutation (Supplementary Figure S7) and was designated *SF3B1* mutant for the differential splicing analysis.

Splice variant analysis in the validation series

The validation set was used to measure the predicted splice variant of 8 genes using specific probes (Supplementary Table 12). 1.3ng of cDNA were analyzed in duplicate to quantify spliced and unspliced forms by real time PCR. 45 cycles of QPCR were conducted on 384 well plates using QuantiTect SYBR Green reagents (Qiagen, Courtaboeuf, France) onto the ABI 9700HT device. To perform the splice variant analysis, 3 steps were achieved per gene of interest. First, CT values were averaged per sample, then a ratio of spliced form was calculated per sample using the formula: $2^{-(\text{CT form1 mRNA - CT form2 mRNA})}$. Finally, for each splicing event, a Mann-Whitney U test was applied between *SF3B1* mutated and wildtype cases.

Statistical methods

Cancer-specific survival (CSS) was calculated from the date of diagnosis to death from uveal melanoma or last follow-up. Event-free survival (EFS) was calculated from the surgical resection to development of metastasis or last follow-up. Survival curves were constructed using the Kaplan–Meier method and the difference between groups was compared with the log-rank test. $\chi 2$ and Fisher's exact tests were used to determine association between variables. P-values less than 0.05 (two-sided) were considered statistically significant.

Data access

Whole genome, RNA-seq and SNP array data have been submitted to the European Genome-phenome Archive (EGA) under study accession number EGAS00001000472.

Supplementary Material

Refer to Web version on PubMed Central for supplementary material.

Acknowledgments

This work was supported by Cancer Research UK (ref: C107/A10433; C5759/A12328), the Wenner-Gren Foundations, Stockholm, Teggerstiftelsen, The Harry J Lloyd Charitable Trust, and The French National Cancer Institute (INCa). We thank Dorine Bellanger and Aurore Rampanou for technical assistance, Aurélie Kamoun for initial splicing analysis and Odette Mariani for managing tumor samples. AGD is supported by the INCa grant “MeluGene".

References

1. Singh AD, Turell ME, Topham AK. Uveal melanoma: trends in incidence, treatment, and survival. Ophthalmology. 2011; 118:1881–5. [PubMed: 21704381]
2. Singh AD, Rennie IG, Seregard S, Giblin M, McKenzie J. Sunlight exposure and pathogenesis of uveal melanoma. Survey of ophthalmology. 2004; 49:419–28. [PubMed: 15231397]
3. Holly EA, Aston DA, Char DH, Kristiansen JJ, Ahn DK. Uveal melanoma in relation to ultraviolet light exposure and host factors. Cancer research. 1990; 50:5773–7. [PubMed: 2393851]
4. Tucker MA, Shields JA, Hartge P, Augsburger J, Hoover RN, Fraumeni JF Jr. Sunlight exposure as risk factor for intraocular malignant melanoma. The New England journal of medicine. 1985; 313:789–92. [PubMed: 4033707]
5. Van Raamsdonk CD, Bezrookove V, Green G, Bauer J, Gaugler L, O'Brien JM, et al. Frequent somatic mutations of GNAQ in uveal melanoma and blue naevi. Nature. 2009; 457:599–602. [PubMed: 19078957]
6. Van Raamsdonk CD, Griewank KG, Crosby MB, Garrido MC, Vemula S, Wiesner T, et al. Mutations in GNA11 in uveal melanoma. The New England journal of medicine. 2010; 363:2191–9. [PubMed: 21083380]
7. Harbour JW, Onken MD, Roberson ED, Duan S, Cao L, Worley LA, et al. Frequent mutation of BAP1 in metastasizing uveal melanomas. Science. 2010; 330:1410–3. [PubMed: 21051595]
8. Martin M, Masshofer L, Temming P, Rahmann S, Metz C, Bornfeld N, et al. Exome sequencing identifies recurrent somatic mutations in EIF1AX and SF3B1 in uveal melanoma with disomy 3. Nature genetics. 2013
9. Harbour JW, Roberson ED, Anbunathan H, Onken MD, Worley LA, Bowcock AM. Recurrent mutations at codon 625 of the splicing factor SF3B1 in uveal melanoma. Nature genetics. 2013; 45:133–5. [PubMed: 23313955]
10. Malcovati L, Papaemmanuil E, Bowen DT, Boultwood J, Della Porta MG, Pascutto C, et al. Clinical significance of SF3B1 mutations in myelodysplastic syndromes and myelodysplastic/myeloproliferative neoplasms. Blood. 2011; 118:6239–46. [PubMed: 21998214]
11. Wang L, Lawrence MS, Wan Y, Stojanov P, Sougnez C, Stevenson K, et al. SF3B1 and other novel cancer genes in chronic lymphocytic leukemia. The New England journal of medicine. 2011; 365:2497–506. [PubMed: 22150006]
12. Biankin AV, Waddell N, Kassahn KS, Gingras MC, Muthuswamy LB, Johns AL, et al. Pancreatic cancer genomes reveal aberrations in axon guidance pathway genes. Nature. 2012; 491:399–405. [PubMed: 23103869]
13. Comprehensive molecular portraits of human breast tumours. Nature. 2012; 490:61–70. [PubMed: 23000897]
14. Quesada V, Conde L, Villamor N, Ordonez GR, Jares P, Bassaganyas L, et al. Exome sequencing identifies recurrent mutations of the splicing factor SF3B1 gene in chronic lymphocytic leukemia. Nature genetics. 2012; 44:47–52.
15. Berger MF, Hodis E, Heffernan TP, Deribe YL, Lawrence MS, Protopopov A, et al. Melanoma genome sequencing reveals frequent PREX2 mutations. Nature. 2012; 485:502–6. [PubMed: 22622578]
16. Turajlic S, Furney SJ, Lambros MB, Mitsopoulos C, Kozarewa I, Geyer FC, et al. Whole genome sequencing of matched primary and metastatic acral melanomas. Genome Res. 2012; 22:196–207. [PubMed: 22183965]
17. Furney SJ, Turajlic S, Stamp G, Nohadani M, Carlisle A, Thomas JM, et al. Genome sequencing of mucosal melanomas reveals that they are driven by distinct mechanisms from cutaneous melanoma. J Pathol. 2013; 230:261–9. [PubMed: 23620124]
18. Pfeifer GP, Besaratinia A. UV wavelength-dependent DNA damage and human non-melanoma and melanoma skin cancer. Photochemical & photobiological sciences : Official journal of the European Photochemistry Association and the European Society for Photobiology. 2012; 11:90–7.
19. Anders S, Reyes A, Huber W. Detecting differential usage of exons from RNA-seq data. Genome Res. 2012; 22:2008–17. [PubMed: 22722343]

20. Shen S, Park JW, Huang J, Dittmar KA, Lu ZX, Zhou Q, et al. MATS: a Bayesian framework for flexible detection of differential alternative splicing from RNA-Seq data. Nucleic acids research. 2012; 40:e61. [PubMed: 22266656]
21. Cazzola M, Rossi M, Malcovati L. Biologic and clinical significance of somatic mutations of SF3B1 in myeloid and lymphoid neoplasms. Blood. 2013; 121:260–9. [PubMed: 23160465]
22. Maciejewski JP, Padgett RA. Defects in spliceosomal machinery: a new pathway of leukaemogenesis. British journal of haematology. 2012; 158:165–73. [PubMed: 22594801]
23. Bonnal S, Vigevani L, Valcarcel J. The spliceosome as a target of novel antitumour drugs. Nature reviews Drug discovery. 2012; 11:847–59. [PubMed: 23123942]
24. Mourskaia AA, Amir E, Dong Z, Tiedemann K, Cory S, Omeroglu A, et al. ABCC5 supports osteoclast formation and promotes breast cancer metastasis to bone. Breast Cancer Res. 2012; 14:R149. [PubMed: 23174366]
25. Alhopuro P, Sammalkorpi H, Niittymaki I, Bistrom M, Raitila A, Saharinen J, et al. Candidate driver genes in microsatellite-unstable colorectal cancer. Int J Cancer. 2012; 130:1558–66. [PubMed: 21544814]
26. Ellis BC, Molloy PL, Graham LD. CRNDE: A Long Non-Coding RNA Involved in CanceR, Neurobiology, and DEvelopment. Frontiers in genetics. 2012; 3:270. [PubMed: 23226159]
27. Graham LD, Pedersen SK, Brown GS, Ho T, Kassir Z, Moynihan AT, et al. Colorectal Neoplasia Differentially Expressed (CRNDE), a Novel Gene with Elevated Expression in Colorectal Adenomas and Adenocarcinomas. Genes & cancer. 2011; 2:829–40. [PubMed: 22393467]
28. Khalil AM, Guttman M, Huarte M, Garber M, Raj A, Rivea Morales D, et al. Many human large intergenic noncoding RNAs associate with chromatin-modifying complexes and affect gene expression. Proc Natl Acad Sci U S A. 2009; 106:11667–72. [PubMed: 19571010]
29. Trapnell C, Roberts A, Goff L, Pertea G, Kim D, Kelley DR, et al. Differential gene and transcript expression analysis of RNA-seq experiments with TopHat and Cufflinks. Nat Protoc. 2012; 7:562–78. [PubMed: 22383036]

Europe PMC Funders Author Manuscripts

Europe PMC Funders Author Manuscripts

Significance

Our data show that despite its dismal prognosis, uveal melanoma is a relatively simple genetic disease characterized by recurrent chromosomal losses and gains and a low mutational burden. We show that *SF3B1* is recurrently mutated in uveal melanoma and the mutations are associated with aberrant alternative splicing.

Europe PMC Funders Author Manuscripts

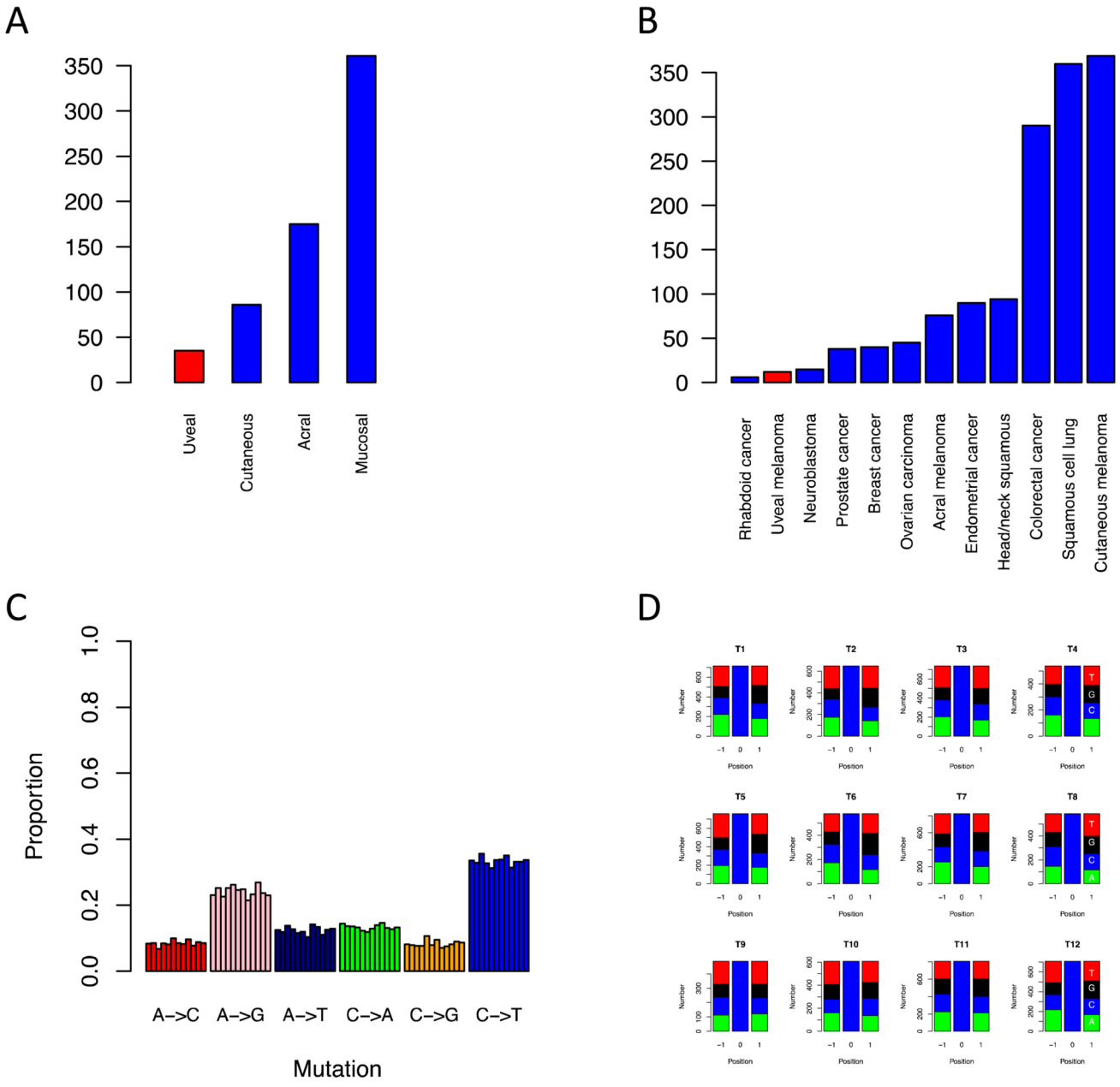

Figure 1. Somatic mutations in uveal melanoma.

(A) Comparison of predicted somatic structural variation in uveal, cutaneous, acral and mucosal melanoma subtypes.

(B) Comparison of non-synonymous point mutation rates identified from whole genome and exome sequencing studies in various solid tumors (Details and references in Supplementary Methods).

(C) Proportion of predicted somatic single nucleotide variants in uveal melanoma genomes by class of mutation.

(D) Frequency of bases ±1 bp of C>T/G>A mutations in the uveal melanoma genomes.

Europe PMC Funders Author Manuscripts

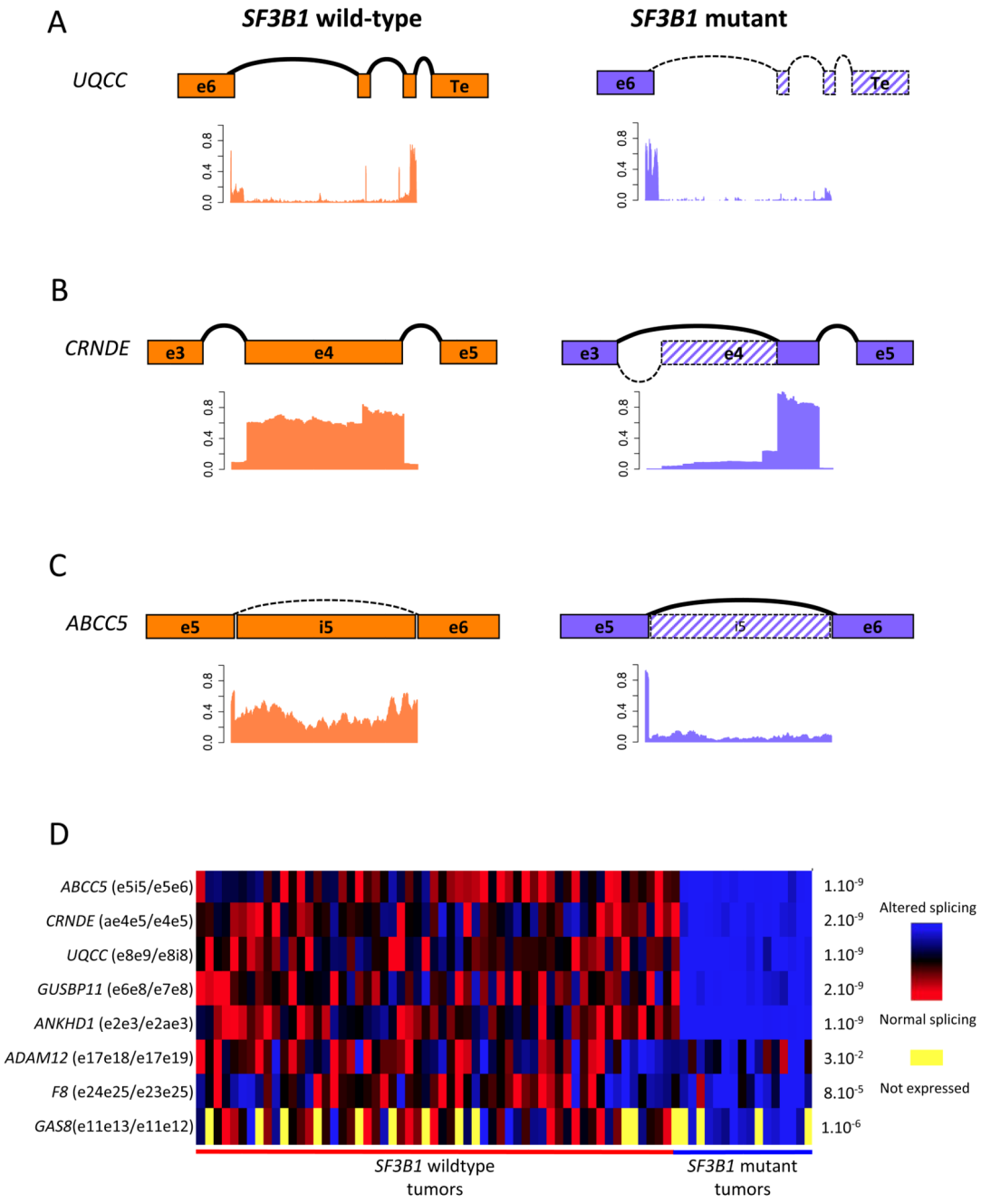

Figure 2. Alternative splicing in SF3B1 mutant uveal melanoma.

(A - C) Plots showing normalized RNA-seq reads for *UQCC* **(A)**, *CRNDE* **(B)** and *ABCC5* **(C)** in *SF3B1* wildtype (orange) and *SF3B1* mutant (mauve) tumors. Above the graphs we show representations of the splicing events. Exons are represented as boxes, with major splicing events indicated by the solid lines/solid boxes and minor splicing by the dotted lines/hashed boxes. Te: terminal exon; e3, e4, e5, e6: exons 3, 4, 5, 6; i5: intron 5.

(D) Heat map of the 8 differentially spliced genes validated by RT-QPCR in a cohort of 74 independent uveal melanoma samples (16 *SF3B1* mutant, 58 *SF3B1* wild-type). The

brackets present the splicing form that was measured, together with exons number involved in each case (e: exon, i: intron, ae: alternative exon). Primer sequences used are presented in Supplementary Table 12 and p-values (Mann-Whitney U test) are indicated without adjustment for the 8 tests. Primary data is shown in Supplementary Fig. S6. Genes that are alternatively spliced are shown in blue; non-spliced genes are shown in red; unexpressed genes are shown in yellow. For each sample, the status of the *SF3B1* gene is indicated.

Europe PMC Funders Author Manuscripts

Europe PMC Funders Author Manuscripts

Table 1

Summary of whole genome sequencing mutations for uveal melanoma.

For each tumor (#1-12), the table shows the total number of predicted SNVs (WGS SNVs), the mutation rate per Mb, the number of coding region SNVs, the total number of predicted indels (WGS indels), and the number of coding region indels.

Tumor #	WGS SNVs	Rate per Mb	Coding region SNVs	WGS indels	Coding region indels
1	2301	0.80	13	178	2
2	2084	0.73	16	62	1
3	2207	0.77	9	52	2
4	1712	0.60	13	49	0
5	2604	0.91	12	93	2
6	1778	0.62	12	47	2
7	2531	0.89	14	89	2
8	1768	0.62	4	48	1
9	1629	0.57	12	56	0
10	1934	0.68	16	72	2
11	2566	0.90	19	102	1
12	2229	0.78	15	86	0

Table 2

Alternative gene splicing associated with *SF3B1* mutations in uveal melanoma.

For each gene indicated, the table presents the prediction of alternative splicing by the GenoSplice EASANA visualization interface in our HTA2 data, and the Harbour *et al.* (9) RNA-Seq data. Also shown is the prediction of these events by DEXSeq and/or MATS in our RNA-Seq data and validation of the events by PCR.

Gene Symbol	Gene Name	Possible Alternative Event (HTA2/GenoSplice EASANA)	Harbour et al. RNA-Seq (GenoSplice EASANA)	Present study RNA-Seq (DEXSeq/ MATS)	RT-qPCR validation
ABCC5	ATP-binding cassette, sub-family C (CFTR/MRP), member 5	Retention of intron 5	√	√	√
CRNDE	Colorectal neoplasia differentially expressed (non-protein coding)	Alternative acceptor site (exon 4)	√	√	√
UQCC	Ubiquinol-cytochrome c reductase complex chaperone	Alternative terminal exons	√	√	√
GUSBP11	Glucuronidase, beta pseudogene 11	Cassette exon 7	√	-	√
ANKHD1	Ankyrin repeat and KH domain containing 1	Alternative acceptors site (exon 3)	√	-	√
ADAM12	ADAM metallopeptidase domain 12	Alternative terminal exons (exon 18 vs. exon 19)	√	-	√
F8	Coagulation factor VIII, procoagulant component	Alternative first exons (exon 23 vs. exon 24)	-	-	√
GAS8	Growth arrest-specific 8	Alternative terminal exons (exon 12 vs. exon 13)	-	-	√